Thermomechanical Analysis for an All-Tungsten ARIES Divertor

James P. Blanchard and Carl Martin
University of Wisconsin, 1500 Engineering Dr., Madison, WI, 53706, blanchard@engr.wisc.edu

The ARIES team is currently proposing two tungsten divertor concepts for their tokamak designs and performed extensive analysis to optimize their thermal and structural performance . Due to the high divertor operating temperatures and the low ductility of tungsten, thermal creep and fracture will be important failure mechanisms to consider. This paper presents a series of finite element analyses addressing the viable operating ranges of these tungsten plate divertor concepts with respect to creep and fracture. For fracture, the J-Integral, a path-independent contour integral that estimates the strain energy release rate for a crack of assumed geometry, is used to address crack propagation. Elliptical surface cracks are introduced both inside and outside the coolant channel and steady state calculations are carried out for both full power and cold shutdown conditions. It is determined that the critical crack is on the inside of the coolant channel with the highest stress intensities at full power operation. Also, transient creep simulations are performed to predict the high temperature thermal deformations and creep strains at various surface flux levels. Finally, transient thermal calculations are carried out to simulate edge localized modes (ELMs) in the plasma, and conclusions are drawn with respect to the severity and frequency of these events with respect to surface melting for the two concepts.

INTRODUCTION

Recent ARIES divertor designs feature two basic concepts: a plate design with a fairly uniform tile geometry spread over a large area, and a "finger" design, which consists of an array of cooling modules distributed over the divertor surface. Extensive analysis and design efforts have been made to ensure that the temperature and stress design requirements at surface heating rates exceeding 10 MW/m^2 [1-7]. These designs, pictured in Fig. 1, are constructed primarily with pure tungsten surface tiles and tungsten alloy structures. The high temperature capability thermal conductivity of tungsten along with the castellated configurations of the plasma facing surfaces enable the divertors to withstand high surface heat fluxes and make the structure tolerant to large transients, such as those caused by ELMS. The material choice carries with it some risk. Tungsten is a relatively low ductility material and thus difficult to machine and susceptible to fracture. Pure tungsten also exhibits creep at relatively moderate temperatures as compared to its melting temperature. In this paper, we explore the mechanics of these components with the goal of establishing the feasibility of using tungsten as a structural material in a high heat flux fusion component. Specifically, we assess the impact of fracture and thermal creep during steady-state and transient operation at various surface flux levels. Finally, the ability to withstand large thermal loading transients such as those associated with ELMS events is investigated with respect to magnitude and frequency of the events and the onset of melting of the tungsten surface.

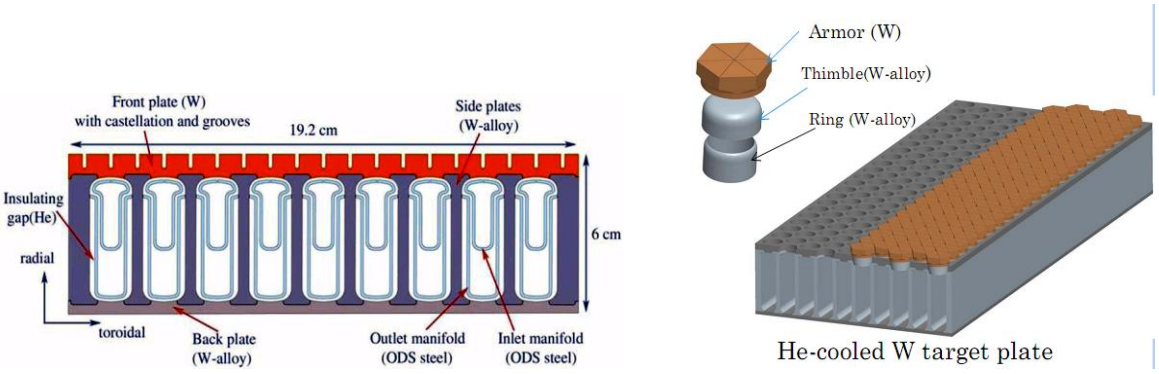

(a) (b)

Fig. 1. Schematic of the ARIES plate divertor cross section. The plate design cross section is shown in (a) and the finger design is shown in (b).

Fracture Analysis for a Generic Design

To explore the viability of tungsten for fusion components, we initially considered fracture in a thin-walled, tungsten tube containing elliptical flaws. The tube diameter (15 mm) and wall thickness (1 mm) corresponded to a T-tube divertor concept under consideration. The cross section of the geometry is shown in Fig. 2. The stress intensity factor was calculated as a function of position on the crack face using ANSYS, a commercial finite element code for an internal pressure load. As shown in Fig. 3, the peak stress intensity was located at the furthest point from the free surface. This analysis was followed by a parametric study of stress intensity factor as a function of crack depth for a pressure of 10 MPa, outer diameter of 15 mm, and wall thickness of 1 mm. As shown in Fig. 4, the stress intensity increases monotonically with crack depth and attains a value of 3 MPa-$m^{1/2}$ for a crack depth of 0.5 mm. In addition, the figure indicates that the stress intensity factor is smaller for circular cracks.

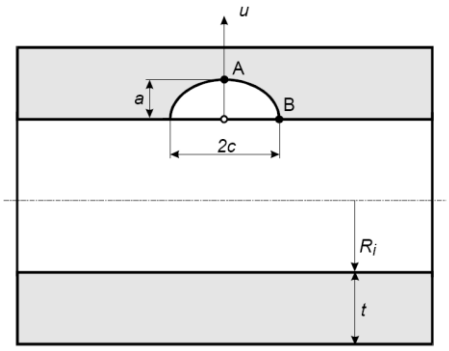

Fig. 2. Cross section of crack geometry for a pressurized tube.

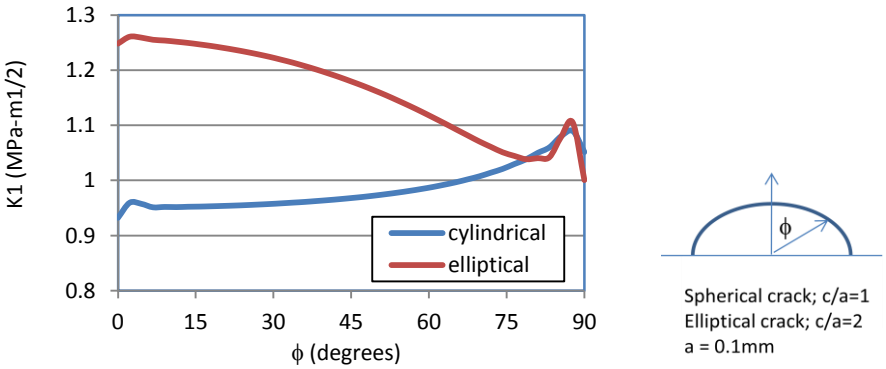

Fig. 3. Stress intensity factor as a function of position along the crack front for a pressurized cylinder.

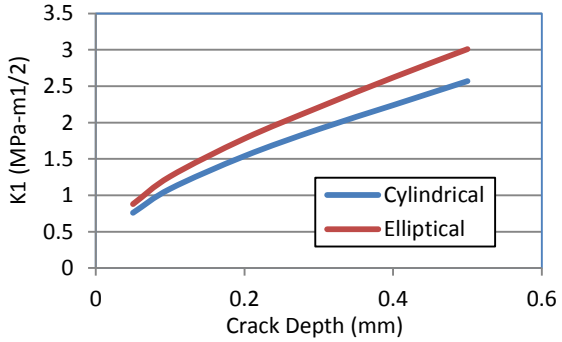

Fig. 4. Stress intensity factor as a function of crack depth for two different crack shapes.

These stress intensity factors can be compared to the fracture toughness of tungsten in order to make an assessment of the viability of the design. The tungsten toughness will vary with the processing of the material prior to and during fabrication, but representative values can be obtained from sintered tungsten [9], as shown in Fig. 5. As shown, the toughness at low temperatures is of the order of the stress intensity factors shown in Fig.4, indicating that the all-tungsten design is feasible, but may have minimal design margin for defects of this size.

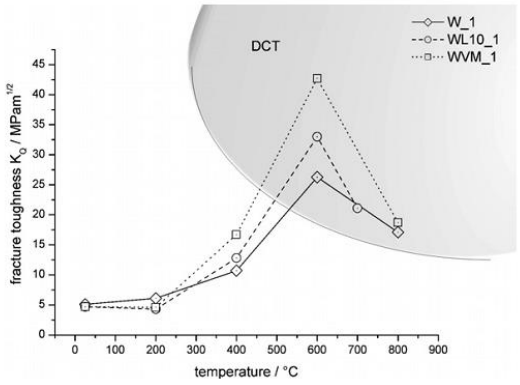

Fig. 1. Fracture toughness of tungsten alloys in the as sintered condition (DCT). The grey area marks the region where linear fracture mechanics is no longer valid.

Fig. 5. Fracture toughness of sintered tungsten [9].

STEADY-STATE THERMAL AND STRUCTURAL ANALYSIS OF THE PLATE DESIGN

A thermal analysis is required to provide temperature inputs to the structural analyses. In this section we present the steady state thermal analysis for the peak heat flux expected in the divertor. The analysis is carried out using ANSYS. 3-D elements are used and a representative section of the component is modeled, employing appropriate boundary conditions to simulate the effects of the surrounding structure and coolant flows. The heating parameters used in the analysis represent a limiting surface heat flux of 11 MW/m^2, and are listed in Fig. 6 along with the resultant structural temperatures. Using these parameters and internal convection conditions gleaned from more complex fluid flow analyses[1], the peak tungsten temperature is found to be 1980 °C in the protective, load free tile region while temperatures in the pressure bearing structural region are below 1300 °C. These temperatures were then transferred to the 3-D structural models. The material models for the structural simulations included both temperature dependent properties and plasticity[8].

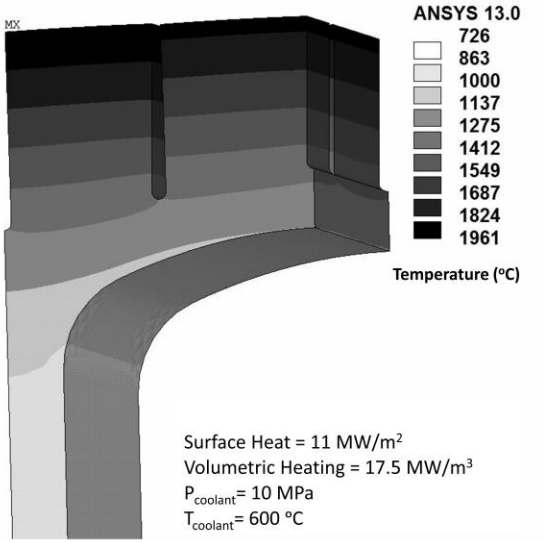

Fig. 6. Steady state full power heating conditions and resulting temperatures (°C).

CRACK-FREE STRESSES

To identify likely locations of critical cracks in the tungsten structure, we first ran a crack-free stress analysis using the previously defined thermal and coolant pressure loads. The stresses in the x-direction (horizontal at the top and perpendicular to the flow direction) are shown in Fig. 7. As shown, the peak tensile stress is on the inside surface of the tungsten and is approximately 484 MPa. The stresses in the direction parallel to the coolant channel (z-direction) are lower than the stresses in the x-direction. Based on this result, a semi-elliptical crack is inserted in the model on the inner surface of the cut face, as shown in Fig. 8.

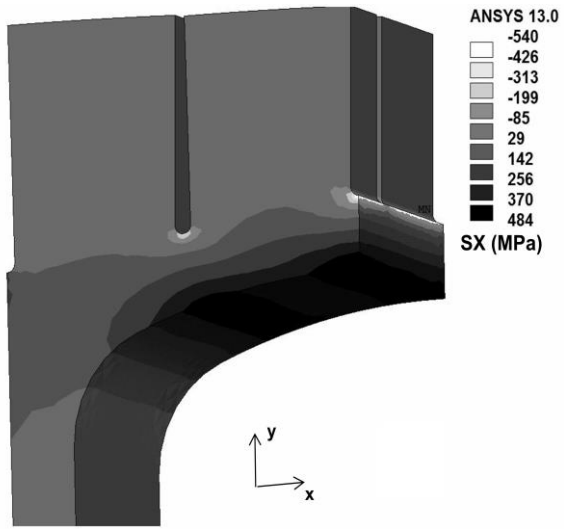

Fig. 7. Thermal and pressure stresses in x-direction.

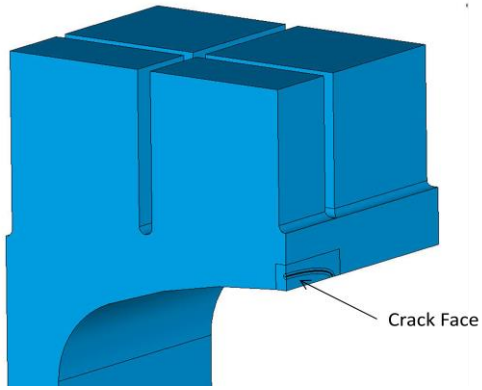

Fig. 8. Crack geometry in initial fracture studies.

FRACTURE MODELING

Fracture is modeled using quarter-point elements at the crack tip (Fig. 9). The J-integral is calculated using a line integral around the crack tip and an equivalent stress intensity factor is calculated for comparison to conventional fracture toughness values. These values are presented parametrically in Fig. 10 for a variety of crack geometries. For reference, the toughness of pure tungsten, Fig. 5, is around 10 MPa-$m^{1/2}$ at 400 °C, though it is fairly sensitive to processing. Additionally, tungsten in the divertor will be subjected to varying degrees of radiation damage which must be accounted for in predicting useful lifetimes.

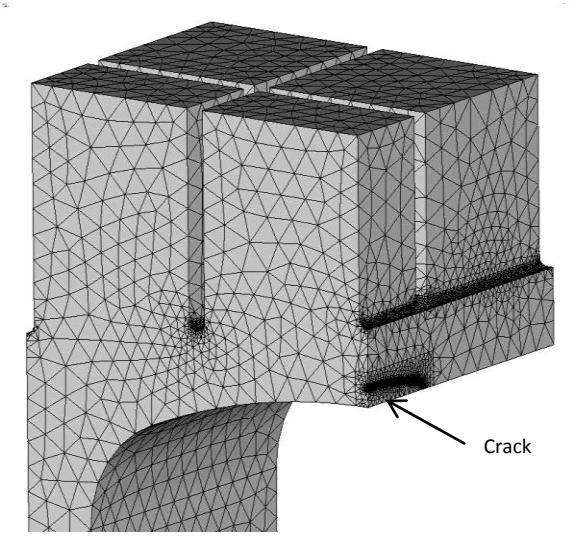

Fig. 9. Close-up view of finite element model showing semi-elliptical crack.

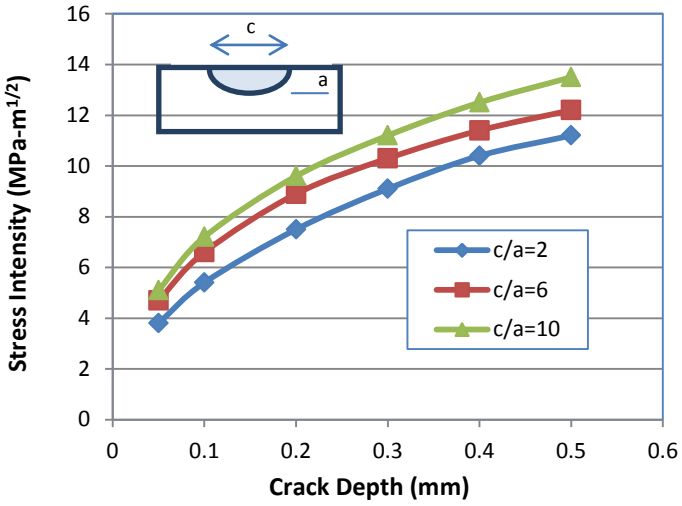

Fig. 10. Stress intensity factor as a function of aspect ratio for a semi-elliptical crack on the inner surface of the divertor for an 11 MW/m^2 surface heat load. In this plot, *c* represents the width of the crack and *a* represents the depth.

Because the thermal surface load of 11 MW/m^2 used to generate the stress intensity curves represents an extreme design case, the stress intensities of a semicircular crack (c/a=2) was explored for a more typical range of heat fluxes. These results, shown in Fig. 11, allow the fracture data to be applied to a wider variety of thermal design points. It can be seen that reducing the surface heat flux from 11 to 4 MW/m^2 reduces the stress intensity for a 0.5 mm crack from 11.4 to 3.8 MPa-m$^{1/2}$. The results for the elliptical cracks would likely be similar.

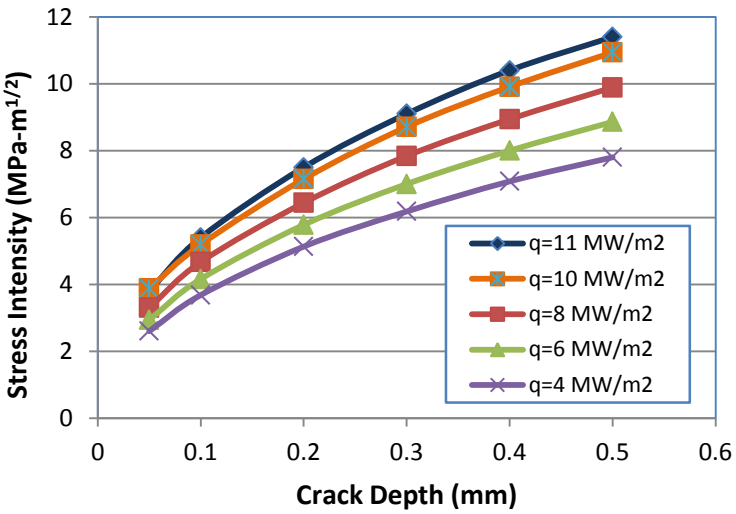

Fig. 11. Stress intensity factor as a function of depth for a semi-circular crack (c/a=2) on the inner surface of the divertor for a range of surface heat loads.

VARYING CRACK LOCATION AND ORIENTATION

As we must determine the crack orientation prior to modeling, other locations must be considered to ensure that we are modeling the critical crack in the structure. To this end, we introduced a crack on the same inner surface of the coolant channel, but rotated 90°. The stress intensity factors for a semicircular crack are shown in Fig. 12. As expected because the stresses normal to the crack face are lower in this orientation, these stress intensities are less severe than those shown in Fig. 10.

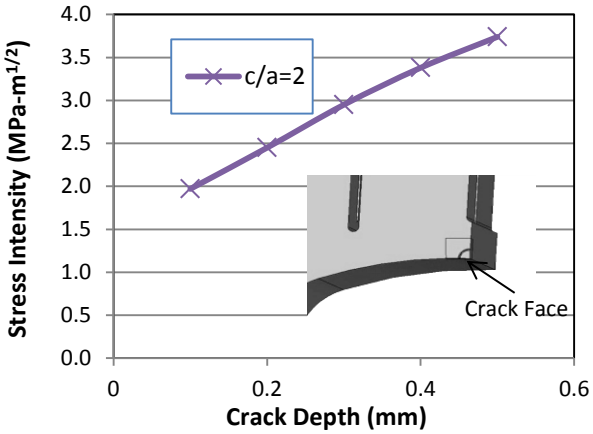

Fig. 12. Stress intensity factors for a crack oriented 90° relative to the crack shown in Fig. 4.

FRACTURE POTENTIAL AT SHUTDOWN

Since there is material yielding and permanent plastic deformation at the region of the highest compressive stress (see Fig. 7) near the notch at the base of the armor. When the heat load is removed and the structure cools, residual stresses will result. These residual stresses will tend to reverse sign relative to the stresses at full power, so one would expect tensile stresses at the notch between tiles after shutdown. For this situation, a crack on the opposite surface, between two tiles was modeled. The location of the crack modeled and the stress intensities calculated for this condition are shown in Fig. 14. The results are for the 11 MW/m^2 surface heat load case, and creep is not considered in the analysis. The stress intensities for this load case are slightly more than half those on the inner surface at full power (Fig. 10).

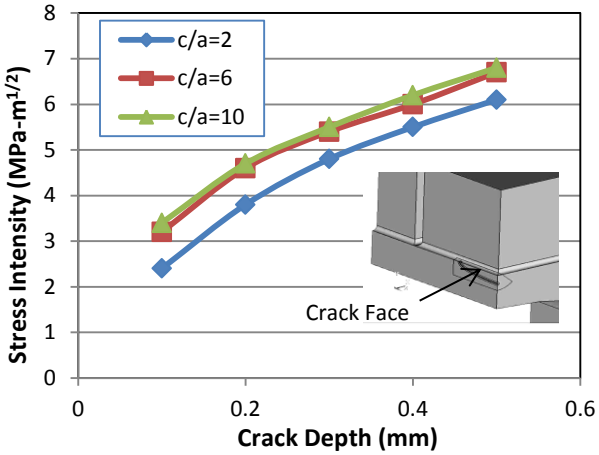

Fig. 14. Stress intensity factors at shutdown for a crack between the tiles.

THERMAL CREEP

Thermal creep is a time-dependent deformation mechanism that is strongly dependent on temperature and stress. The deformation tends to be damaging to the structural materials and hence it is often the life-limiting failure mechanism at high temperatures. To assess the effect of thermal creep on the ARIES divertor life assessment, we have incorporated thermal creep into our finite element models for the plate divertor and run time dependent analyses with constant heat loads. As tungsten is most often used for light bulb filaments and heating elements, available creep data tends to be for higher temperatures and lower stress levels, and data for the temperatures and stress ranges of interest in this study are limited. Creep data for tungsten in the temperature range (1000 - 1400 °C) [10] were fit to a power law creep model resulting in the following:

$$\dot{\epsilon} = 156 \left[e^{\frac{-53370}{T}} \right] \sigma^5 \qquad (1)$$

where $\dot{\epsilon}$ is the creep rate (hr^{-1}), σ is the stress (MPa) and T is the temperature (°K). Hence, small design changes can have dramatic impacts on the stress and deformation results. Initial runs with this model assumed steady state conditions and applied the maximum 11 MW/m^2 surface heat flux on the divertor surface. The model was run for 18000 hours and the displacement at the center of the coolant channel is shown in Fig. 18. These displacements (5 mm) are excessive and are accompanied by very high creep strains. In order to better understand the viable operating heat flux range of this divertor concept, the maximum out-of-plane displacement after two years of operation as a function of heat flux are plotted in Fig. 16. The maximum out-of-plane displacement begins to rise rapidly for fluxes above 8 MW/m^2.

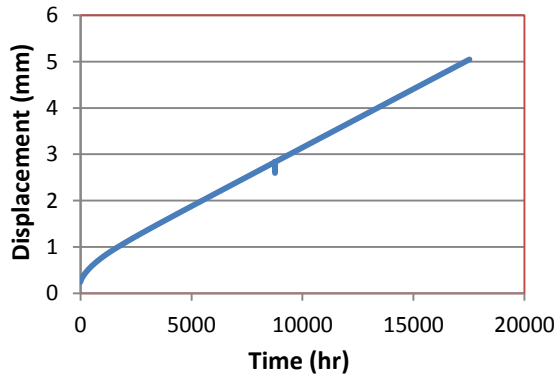

Fig. 15. Maximum divertor front plate out-of-plane displacement for nominal 11 MW/m^2 steady-state heat and 10 MPa pressure loads.

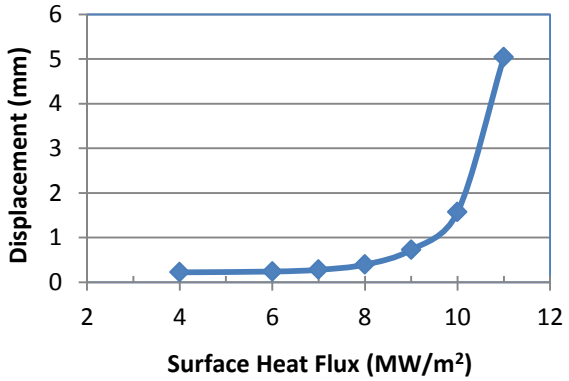

Fig. 16. Maximum divertor front plate out-of-plane displacement after 2 years as a function of surface heat flux.

To reduce the thermal creep rates in this structure, we must reduce either the stress or the temperature. To reduce the stress, the pressure is the key parameter, because the secondary thermal stresses relax out and do not contribute in any significant way to the long-term, accumulated creep strains. To reduce the temperature, one can lower the bulk coolant temperature (though this will decrease the difference between the minimum structure temperature and the recrystallization temperature of the tungsten) or reduce the surface heat flux. To explore this effect the surface heat flux was reduced from 11 MW/m^2 to a more typical divertor flux of 6.7 MW/m^2. This reduces the peak surface temperature from 1980 °C to 1433 °C and the maximum temperature of the pressure bearing structure to 1020 ^{o}C. Due to the nonlinearity of the creep relation, creep rates are dramatically reduced. As shown in Fig. 17, the peak creep strains after two years are less than 0.1%, which is below the allowable amount. Also in this figure are results for pressure only (thermal expansion set to zero) and thermal only (pressure set to zero) creep analyses. These show the stress relaxation (saturation of thermal creep strain) of the thermal stresses and the long-term impact of the pressure stresses. Also worth noting is that the sum of the thermal and pressure creep components is much less than the total creep and the high creep rates early in the time history when the thermal and pressure stresses add. This highlights the nonlinearity of the creep rate with stress (σ^5).

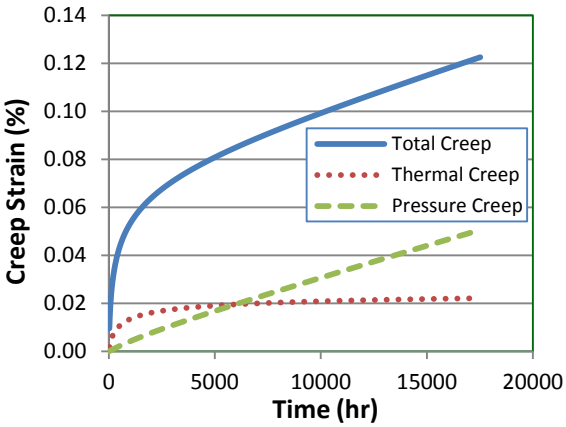

Fig. 17. Creep strains after two years for three cases: pressure loading only, thermal loading only, and both loads together. These results are for a location on the inner surface of the coolant channel, near the top.

The sensitivity of this creep strain to variations in the surface heat flux and the coolant pressure are shown in Fig. 18. In either case, the baseline load is varied about the baseline value and the normalized creep strain is plotted as a function of the varying parameter (normalized to the baseline value). Again, the rapid increase in creep strain with increasing heat rate, and hence structural temperature, is apparent above the nominal 6.7 MW/m^2 heat flux (maximum structural temperature 1020 ^{o}C).

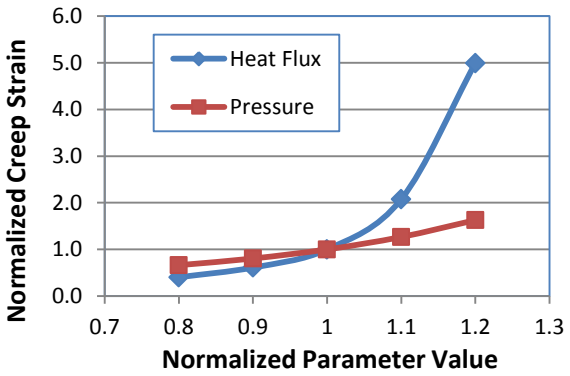

Fig. 18. Normalized variation in peak creep strain for different values of the surface heat flux and coolant pressure. The baseline flux and pressure are 6.7 MW/m^2 and 10 MPa.

Finally, the depth of the notch between tiles was varied to assess the impact on the creep rate. This modification effectively reduces the tile thickness and increases the upper channel wall thickness, thus increasing the thermal stress and decreasing the pressure stress. As shown in Fig. 19, reducing the notch depth from 5 mm to 4 mm, effectively increasing outer wall thickness from 2 mm to 3 mm, decreases the creep strain after two years by about 23%.

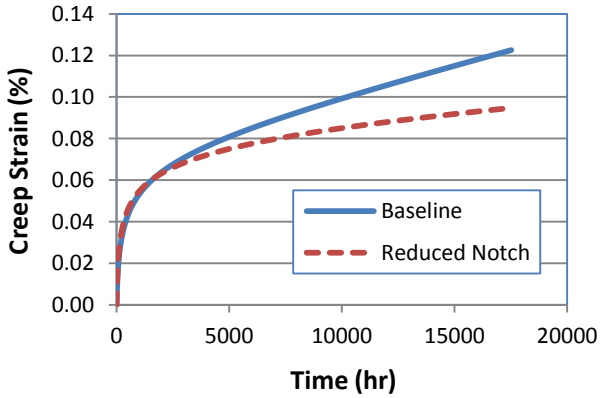

Fig. 19. Creep strain over a two year period for the nominal design and a design with a reduced depth notch.

It is also instructive to observe the time-dependent stresses in a creep situation. The stresses associated with the results described above are plotted in Fig. 20 for two points on the divertor channel wall. As can be seen, thermal stresses will relax out due to thermal creep deformation (and the stresses will reverse on shutdown), but pressure stresses are required for the maintenance of equilibrium and cannot be relaxed out. Hence, it is the primary stress field due to the coolant pressure that will tend to be life-limiting where creep is a concern.

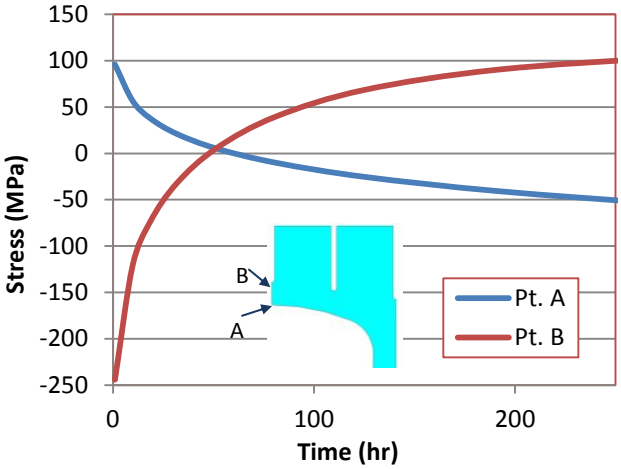

Fig. 20. Stresses as a function of time at two points on the divertor channel. Thermal stresses are relieved by creep strains.

THERMAL TRANSIENTS

Plasma-facing structures are expected to experience transient heat loads that will complicate their failure analysis and design. As an example, consider edge-localized modes (ELMs), which deposit heat on those surfaces in bursts. To address the implications of ELMS, we must address both sub-surface and surface effects. To estimate the importance of sub-surface effects, we applied a transient heat load with a triangular pulse shape for 20 cycles to the divertor surface and observed temperature fluctuations at the surface and 2.5 mm below the surface. In this simulation, the peak divertor heat flux was varied +/- 20%, a far smaller fluctuation than one would expect in a typical ELM. However, it still permits conclusions regarding the relative importance of these transients to temperature and stress fluctuations below the surface. As shown in Fig. 21, this simulation exhibits a fluctuation of approximately 3.5° at the surface, while there is no detectable fluctuation 2.5 mm below the surface. Hence, we conclude that ELMs with a 1 ms pulse width are not expected to cause subsurface failure in these structures.

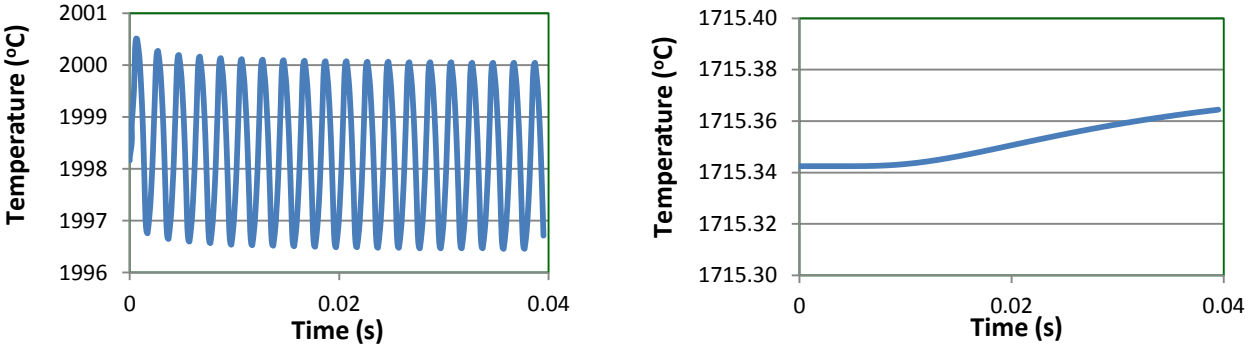

(a) (b)

Fig. 21. Temperature variation at surface (a) and 2.5 mm below the surface (b) as a result of a triangular heat pulse with peak variations of +/- 20% of the nominal heat flux.

To better simulate the surface effects of ELMs, we must use a more realistic estimate of the heat load variations. More specifically, It is predicted that the divertor structures will experience steady state surface heat loads of 6.7 MW/m^2 with intermittent spikes from ELM events of approximately 1.95 MJ spread over a surface area of 1.44 m^2 with a triangular heat pulse with a 0.4 ms rise time and a 0.8 ms fall time.[11] The average ELM heat flux is thus 1128 W/m^2 over the 1.2 ms event with the peak flux twice that value. The divertor model begins with a steady state temperature distribution from the 6.7 MW/m^2 surface flux followed by the ELM load to the surface for a single pulse. The time-dependent temperatures resulting from this simulation are shown in Fig. 22. Temperatures in this analysis exceed the tungsten melting point, so the model was modified to incorporate the latent heat of fusion for tungsten. As can be seen in this figure, this ELM load will melt

approximately 20 microns of the surface, given the 3410 °C melting temperature of pure tungsten. Further design considerations are necessary to explore options for eliminating melting during these events.

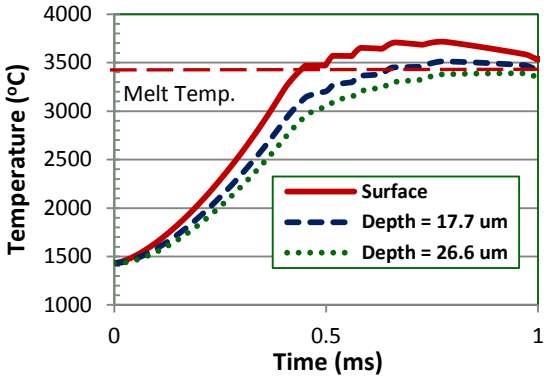

Fig. 22. Time-dependent temperatures near the divertor surface resulting from a single ELM load.

Given the uncertainty in the loads during a series of ELM events, including uncertainty in both the inter-ELM heat flux and the ELM heat load and frequency, we have carried out a series of parametric studies to assist in future design decisions. The inter-ELM heat flux was varied between 2 and 10 MW/m^2 and the maximum allowable ELM heat load to reach the melt threshold were determined iteratively. These results were generated for single ELM events and repeated events at 5 Hz and 10 Hz rates and are summarized in Fig. 23. From this figure, for a divertor with a steady state surface heat load of 6.7 MW/m^2, a single ELM event will likely produce melting if the average heat flux exceeds 800 MW/m^2 while repeated ELMs at a 10 Hz rate would cause melting if the average flux exceeds 480 MW/m^2. This compares with the average ELM heat flux of 1128 W/m^2 in the initial estimate that produced about 20 microns of surface melting.

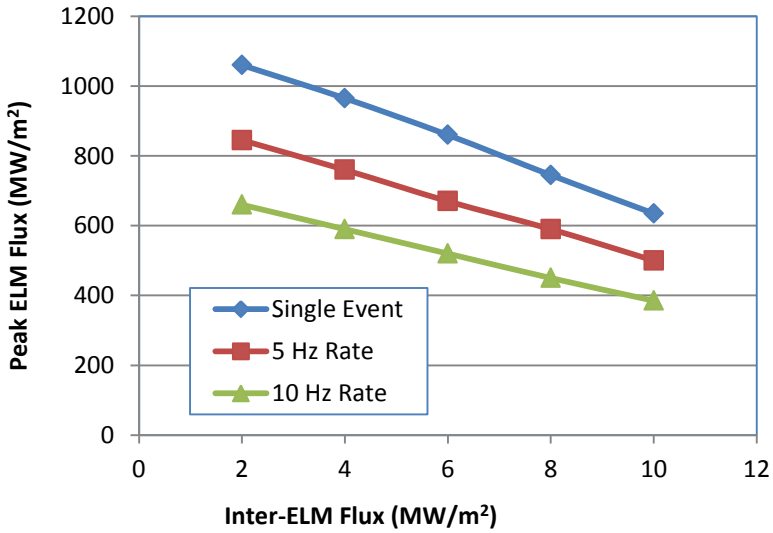

Fig. 23. Melting thresholds for combinations of inter-ELM heat flux and average heat flux during the ELM at different frequencies for plate divertor.

TRANSIENTS IN THE FINGER DESIGN

The second divertor concept, the finger design, is being developed for higher heat load regions and has been proposed for heat fluxes up to 15 MW/m^2. The hexagonal castellated tiles mounted on individual thimbles, Fig. 24, with multiple impinging cooling jets maximize heat transfer and minimize thermal stress. This design potentially offers greater tolerance to the extremes of ELM events. In order to investigate their performance a similar melt threshold analysis was performed for the finger concept as for the plate divertor. In order to facilitate the numerous analyses required for this, the hexagonal tiles were simulated with an axisymmetric FEA model, and the complex interior cooling from the multiple jets were replaced with averaged convection coefficients. The temperature results for a 10 MW/m^2 steady surface heat flux were benchmarked against 3-D fluid thermal results. Temperatures from the axisymmetric model along with relevant heat transfer inputs are illustrated in Fig. 25.

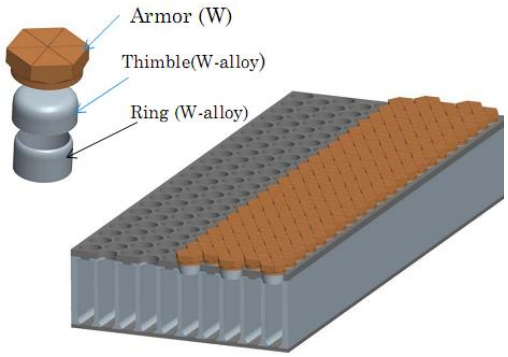

Fig. 24. Schematic of the finger design divertor concept for ARIES.

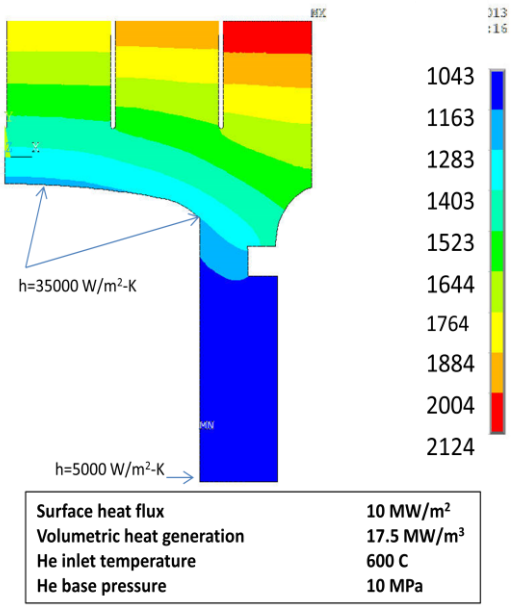

Fig. 25. Temperatures (^{o}C) from the axisymmetric finger FEA model and relevant heat transfer inputs.

The finger concept, because of its higher design flux capability as compared with the plate concept, might potentially be more tolerant of the severe transient loadings characteristic of ELM events. To investigate this, the parametric melt limit analysis of the combined inter-ELM and transient ELM loading was repeated for the finger concept. These results are plotted in Fig. 26 and compared with the plate divertor concept in Fig. 27. From Fig. 27, the finger concept offers only marginal

improvement in tolerating ELM events without melting which is rather surprising since the finger design is designed to operate under steady state fluxes up to 40% higher than the plate design. The finger design's hexagonal shape, while minimizing thermal stress and limiting structural temperatures, has quite similar maximum operating surface temperatures under equivalent heat fluxes as the plate design. So for this analysis, which considers only the onset of surface melting, the finger design does not offer the higher flux capability that is seen for steady state conditions.

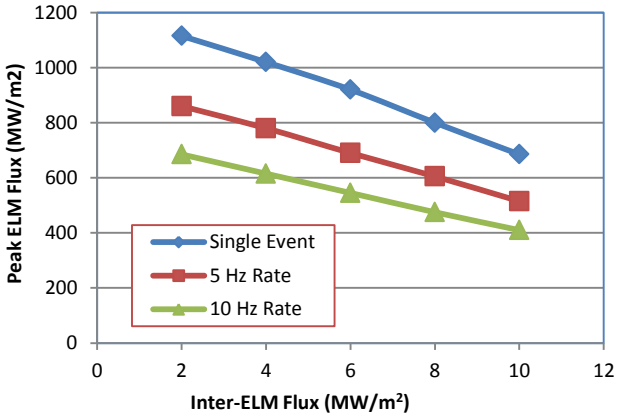

Fig. 26. Melting thresholds for combinations of inter-ELM heat flux and average heat flux during the ELM at different frequencies for finger divertor.

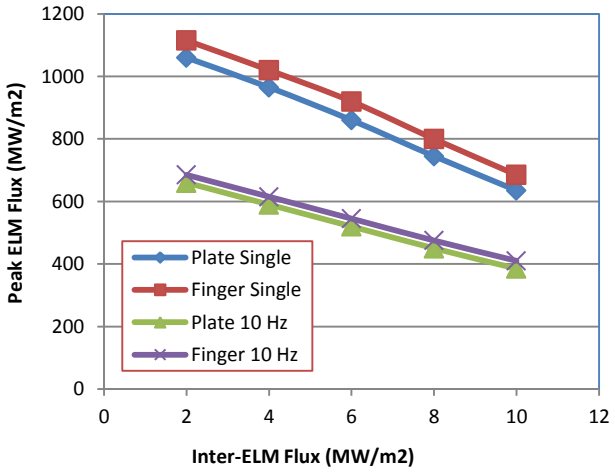

Fig. 27. Comparison of the melting thresholds ELM combinations for plate and finger divertor concepts.

CONCLUSIONS

A series of analyses are carried out to assess the performance of tungsten divertor designs in a tokamak with respect to fracture, creep , and extreme thermal transients. Fracture analyses indicated that the ARIES divertor design can tolerate cracks of sufficient size to be detectable prior to operation. Thermal creep rates have been investigated at a range of operating conditions. Again, preliminary calculations indicate that, without prudent design, creep rupture will likely lead to failure at the extreme ends of the operating ranges proposed for theses. Parametric studies indicate that there are several options for design changes that will alleviate creep damage, and more material data is required for both fracture toughness and creep rates under the applicable temperature and stress ranges is need. Finally, preliminary analysis of edge-localized modes indicates melting of the divertor surface, but design changes are under consideration that may alleviate the surface damage.

ACKNOWLEDGMENTS

Funding has been provided by the Department of Energy: #DE-FG02-98ER54462

REFERENCES

1. X.R. Wang et al, "Design Optimization of High-Performance Helium-Cooled Divertor Plate Concept," *Fusion Science & Technology*, **56**, 2009.
2. X.R. Wang, S. Malang, M. S. Tillack, J. Burke and the ARIES Team, "Recent Improvements of the Helium-Cooled W-based Divertor for Fusion Power Plants," *Fusion Engineering and Design*, **82,** 2012.
3. X.R. Wang, S. Malang and M.S. Tillack, "High performance Divertor Target Concept for a Power Plant: A Combination of Plate and Finger Concepts," *Fusion Science & Technology*, **60**, 2011.
4. D. Navaei, X.R. Wang, M.S. Tillack and S. Malang, "Elasto-plastic Analysis of the Transition Joint for High Performance Divertor Target Plate," *Fusion Science & Technology*, **60**, 2011.
5. M.S. Tillack, A.R. Raffray, X.R. Wang, S. Malang, S. Abdel-Khalik, Y. Minami, and D. Youchison, "Recent US Activities on Advanced He-Cooled W-Alloy Divertor Concepts for Fusion Power Plants," *Fusion Engineering and Design*, **86**, 2011.
6. X.R. Wang, S. Malang and A.R. Raffray, "Transient Thermal and Stress Response of A Helium-Cooled Tungsten Plate-Type Divertor," *Proceedings of the 23rd Symposium on Fusion Engineering*, 2009.
7. A.R. Raffray, S. Malang, X.R. Wang, "Optimizing the overall configuration of a He-cooled W-alloy divertor for a power plant," *Fusion Engineering and Design*, **84**,2009.
8. J. Blanchard and C. Martin, Thermomechanical Effects in a Laser IFE First Wall, J Nuc Mat, 347 (3), 2005.
9. B. GLUDOVATZ et al, "Fracture Toughness of Polycrystalline Tungsten Alloys," 17th Plansee Seminar, 2009.
10. Pugh, J. W., "Tensile and Creep Properties of Tungsten at Elevated Temperatures," Proc. ASTM, vol. 57, 1957.
11. C. T. Kessel et al, "The Evaluation of the Heat Loading From Steady, Transient and Off-Normal Conditions in ARIES Power Plants," to appear in *Fusion Science and Technology* (2013).